Atmos. Chem. Phys. Discuss., 11, 1595–1639, 2011
www.atmos-chem-phys-discuss.net/11/1595/2011/
doi:10.5194/acpd-11-1595-2011

Atmospheric Chemistry and Physics Discussions

Simulated enhancement of ENSO-related rainfall variability due to Australian dust

L. D. Rotstayn[1], M. A. Collier[1], R. M. Mitchell[2], Y. Qin[2], and S. K. Campbell[2]

[1]Centre for Australian Weather and Climate Research, CSIRO Marine and Atmospheric Research, Aspendale, Vic, Australia
[2]Centre for Australian Weather and Climate Research, CSIRO Marine and Atmospheric Research, Canberra, ACT, Australia

Received: 20 December 2010 – Accepted: 12 January 2011 – Published: 19 January 2011

Correspondence to: L. D. Rotstayn (leon.rotstayn@csiro.au)

Published by Copernicus Publications on behalf of the European Geosciences Union.

Abstract

Average dust emissions from Australia are small compared to those from the major sources in the Northern Hemisphere. However, they are highly episodic, and this may increase the importance of Australian dust as a climate feedback agent. We compare two 160-year coupled atmosphere-ocean simulations of modern-day climate using the CSIRO Mark 3.6 global climate model (GCM). The first run (DUST) includes an interactive treatment of mineral dust and its direct radiative effects. The second run (NODUST) is otherwise identical, but has the Australian dust source set to zero. We focus on the austral spring season, when the correlation between rainfall and the El Niño Southern Oscillation (ENSO) is strongest over Australia. We find that the ENSO-rainfall relationship over eastern Australia is stronger in the DUST run: dry (El Niño) years tend to be drier, and wet (La Niña) years wetter. The ENSO-rainfall relationship is also weaker over north-western Australia in the DUST run. The amplification of ENSO-related rainfall variability over eastern Australia and the weaker ENSO-rainfall relationship over the north-west both represent an improvement relative to observations. The suggested mechanism over eastern Australia involves stabilisation of the surface layer due to enhanced atmospheric heating and surface cooling in El Niño years, and enhanced ascent and moisture convergence driven by atmospheric heating in La Niña years. The results suggest that (1) a realistic treatment of Australian dust may be necessary for accurate simulation of the ENSO-rainfall relationship over Australia, and (2) radiative feedbacks involving dust may be important for understanding natural rainfall variability over Australia.

1 Introduction

Mineral dust is both strongly influenced by climate and itself influences climate. Dust aerosols exert substantial direct effects by scattering and absorbing shortwave radiation and absorbing longwave radiation (Satheesh and Moorthy, 2005). In addition to

ACPD
11, 1595–1639, 2011

these direct effects, dust affects cloud microphysics and the efficiency of precipitation formation (Wurzler et al., 2000; Rosenfeld et al., 2001). It also provides an important biogeochemical link between terrestrial and marine ecosystems (Ridgwell, 2002). Dust is an important vector for iron supply to the ocean, which subsequently impacts ocean productivity, atmospheric CO_2 concentrations, and hence global climate (Mackie et al., 2008).

Regionally, dust can exert large radiative effects, especially on surface shortwave radiation. For example, Haywood et al. (2003) estimated a maximum decrease of short wave radiation at the surface of 209 $W\,m^{-2}$ during a dust event over the North Atlantic Ocean in September 2000. As a partially absorbing aerosol, dust also tends to increase atmospheric stability and reduce convection (Satheesh and Moorthy, 2005). However, the reality is more complex, because the forcing and response to absorbing aerosols can depend strongly on their relationship to clouds (Liao and Seinfeld, 1998), their optical properties (Miller et al., 2004), altitude (Penner et al., 2003) and the aridity of the environment (Miller et al., 2004).

Climatic conditions strongly influence atmospheric dust concentration, via their effects on dust emission, transport and deposition. For example, transport of African dust across the North Atlantic shows large interannual changes that are highly anti-correlated with rainfall in the Soudano-Sahel region (Prospero and Lamb, 2003). Wind erosion of soils is sensitive to vegetation cover and soil moisture, as well as the intrinsic properties of the soil (Gillette and Passi, 1988; Fécan et al., 1999; Webb et al., 2006; Ishizuka et al., 2008). Zender and Kwon (2005) found that, in most regions, precipitation and vegetation variations strongly constrain dust anomalies, with dust emission and precipitation being negatively correlated on multiple timescales. However, in some regions dust and precipitation anomalies correlate positively. This can occur where flood-transported sediments increase dust emission during subsequent dry periods (McTainsh et al., 1999).

These effects create the possibility of large feedbacks between dust and regional climate variations. Saharan dust-induced surface cooling and lower atmospheric heating

ACPD
11, 1595–1639, 2011

has been shown to increase atmospheric stability and reduce convection in the tropical Atlantic Ocean; this may explain the strong inverse relationship between inter-annual variations of tropical cyclone activity and Saharan dust outbreaks (e.g., Evan et al., 2006; Sun et al., 2009). Model simulations suggest that direct radiative forcing by increased levels of North African dust can explain up to 30% of the observed precipitation reduction in the Sahel between wet and dry periods (Yoshioka et al., 2007). Modelling of the 1930s "dust bowl" drought in North America suggests that human-induced land degradation is likely to have contributed to the dust storms and also amplified the drought, in part due to the direct radiative effects of dust (Cook et al., 2009).

Australia is the dominant source of dust in the Southern Hemisphere (Tanaka and Chiba, 2006; Mackie et al., 2008). Satellite retrievals identify the large (1 140 000 km^2) Lake Eyre Basin of central-eastern Australia as the largest dust source in the Southern Hemisphere (Prospero et al., 2002); see also Washington et al. (2003), McTainsh et al. (2007), Bullard et al. (2008) and Mitchell et al. (2010). Compared to the major Northern Hemisphere dust source regions, Australian average dust emissions are relatively low. However, they are very episodic, with periods of high dust activity occurring during drought (McTainsh et al., 2007). Australia's Southern Hemisphere location and the sensitivity of its responses (in both time and space) to rainfall variations may increase the importance of Australian dust as a feedback on climate.

To our knowledge, there have been no modelling studies of the direct radiative effects of Australian dust on climate. However, Rotstayn et al. (2010) noted a substantial improvement in the simulation of Australian natural rainfall variability in an updated version of the CSIRO global climate model (GCM), which they tentatively attributed to the inclusion of an interactive dust treatment. They assessed the model's simulation of the leading modes of annual rainfall variability using empirical orthogonal teleconnections (EOTs; van den Dool et al., 2000). Compared to its predecessor (Mark 3.5), the updated model (Mark 3.6) was better able to capture the spatial pattern of the leading rainfall mode, which represents variability due to the El Niño Southern Oscillation (ENSO). In Mark 3.6, the ENSO-related rainfall mode was centred over eastern

ACPD
11, 1595–1639, 2011

Australia, in good agreement with observations, whereas in Mark 3.5 it was incorrectly centred over Western Australia.

Based on qualitative arguments, Rotstayn et al. (2010) proposed that by further suppressing convection over eastern Australia during El Niño events (and enhancing it during La Niña events), dust feedbacks may increase the magnitude of rainfall variability there, in tune with the model's ENSO cycle. However, because their updated model included other changes besides the inclusion of an interactive dust scheme, they were unable to state this with confidence. An accurate simulation of this rainfall mode is necessary for modelling the response of Australian rainfall to anthropogenic climate change. The hypothesis also suggests that feedbacks involving dust may be important for understanding natural rainfall variability over Australia. For example, it is possible that there is a positive feedback on drought induced by the recent observed increase in Australian dust (Mitchell et al., 2010).

The purpose of this paper is to investigate the effect of Australian dust on ENSO-related rainfall variability by comparing two coupled ocean-atmosphere simulations with the CSIRO Mark 3.6 GCM (hereafter Mk3.6). The first is an extension of the run described by Rotstayn et al. (2010), with the Australian dust source included. The second run is otherwise identical, but the Australian dust source is set to zero. By comparing two runs which differ on only one respect, it should be possible to isolate the effect of Australian dust.

An outline of the paper is as follows. In Sect. 2, the model and simulations are described. Section 3 presents the dust simulation, observed and modelled ENSO-rainfall relationships, and discussion of a possible mechanism for the dust-ENSO radiative feedback. Section 4 contains conclusions.

ACPD
11, 1595–1639, 2011

2 Model and simulations

2.1 Model description

The CSIRO Mk3.6 GCM is described by Rotstayn et al. (2010). It was developed from the earlier Mk3.5 version (Gordon et al., 2010); for an historical overview see Smith (2007). It is a coupled ocean-atmosphere model with dynamic sea ice, and horizontal resolution of approximately $1.9^{\circ} \times 1.9^{\circ}$ (spectral T63). The atmospheric component has 18 vertical levels. The main differences between Mk3.5 and Mk3.6 are the incorporation of an interactive aerosol treatment and an updated radiation scheme in the latter. The aerosol species treated interactively are sulfate, black carbon, organic aerosol, mineral dust and sea salt. All the above aerosol types, except for sea salt, are treated prognostically by the model, so that equations are included for their emission, transformation, transport and removal at each time step. In all, there are 11 prognostic variables in the aerosol scheme: dimethyl sulfide (DMS), sulfur dioxide (SO_2), sulfate, hydrophobic and hydrophilic forms of black carbon and organic aerosol, and four size bins of mineral dust, with radii ranging from 0.1–1, 1–2, 2–3 and 3–6 μm respectively. A further two modes of sea salt are diagnosed as a function of wind speed in the marine boundary layer, but are not treated prognostically. Also, the distribution of stratospheric aerosol from volcanic eruptions is prescribed using monthly mean data (extended from Sato et al., 1993). Rotstayn et al. (2007) give further details of the aerosol schemes (including their limitations). The aerosol treatments are supported by an updated radiation scheme that includes aerosol-radiative effects (Grant et al., 1999; Chou and Lee, 2005; Rotstayn et al., 2007). The radiation scheme treats the shortwave effects of all the above aerosol types and the longwave effects of dust and volcanic aerosol. Indirect effects of aerosol on liquid-water clouds depend only on sulfate, carbonaceous aerosol and sea salt (Rotstayn et al., 2010), and it should be noted that indirect effects of dust are not included in the model.

The treatment of mineral dust emission follows Ginoux et al. (2001, 2004). The scheme is based on satellite retrievals from the Total Ozone Monitoring Spectrometer

ACPD
11, 1595–1639, 2011

(TOMS), which indicate that most major dust sources correspond to topographic depressions (Prospero et al., 2002). These are typically dry lakes or riverbeds where a sufficiently deep layer of loose alluvial sediment was able to accumulate. Zender et al. (2003) found that assigning enhanced erodibility to topographic minima (as in Ginoux et al., 2001) realistically increases emissions in several regions, including the Lake Eyre basin in central-eastern Australia. The characterisation of the Lake Eyre basin as the major Australian dust source is also broadly consistent with several studies cited in the Introduction. The dust source function depends on the prescribed spatial distribution of soil erodibility for each dust size class and a threshold value of 10-metre wind speed (u_{10m}). Above this threshold wind speed u_t, which is a function of soil moisture, the dust source is proportional to $u_{10m}^2(u_{10m} - u_t)$; see Ginoux et al. (2004).

To account for mesoscale variations that are unresolved on the relatively coarse grid of our GCM, our dust emission scheme includes a parameterization of sub-grid gustiness due to deep convection and boundary-layer free convection, based on Redelsperger et al. (2000). The term related to deep convection is (in m s^{-1})

$$V_{\text{deep}} = \left(\frac{19.8R^2}{1.5 + R + R^2)} \right)^{0.4} \quad (1)$$

where R is the rainfall rate in cm per day. The term related to free convection is

$$V_{\text{free}} = 0.65 w_* \quad (2)$$

where w_* is the free convection velocity (Deardorff, 1970). As noted by Lunt and Valdes (2002), these terms can plausibly be added in quadrature, or linearly, with the latter giving a larger effect. In the current version of our model, the terms are added linearly, so that the effective wind speed used in the dust emission scheme is

$$V_{\text{eff}} = V_{10} + V_{\text{deep}} + V_{\text{free}} \quad (3)$$

where V_{10} is the grid-resolved 10-metre wind speed.

ACPD
11, 1595–1639, 2011

Transport of dust occurs by advection, vertical turbulent mixing and vertical transport inside deep convective clouds. Vertical advection is handled using a flux-corrected transport scheme (Van Leer, 1977), and horizontal advection is handled via a semi-Lagrangian scheme (McGregor, 1993). The treatment of vertical turbulent mixing is based on stability-dependent K-theory (Louis, 1979). Under convective conditions, an additional non-local counter-gradient flux is added (Holtslag and Boville, 1993). Convective transport is based on the vertical profiles of the updraft mass flux and compensating subsidence generated by the convection scheme (Gregory and Rowntree, 1990).

Removal of dust from the atmosphere occurs via wet and dry deposition and gravitational settling. Wet deposition is linked to the formation of warm rain and frozen precipitation in the stratiform-cloud and convection schemes (Rotstayn and Lohmann, 2002). The treatment of dry deposition and gravitational settling is described by Ginoux et al. (2001).

The model's dust optical properties were revised by Rotstayn et al. (2010), to improve the shortwave treatment and to include longwave effects, which were previously omitted. The refractive indices used to derive the shortwave optical properties were revised due to mounting evidence from observations that older models tend to overestimate the absorption of shortwave radiation by dust (Myhre et al., 2003; Yu et al., 2004). The revised scheme uses refractive indices based on measurements at Bahrain (Dubovik et al., 2002); these have smaller imaginary components than the old refractive indices, giving less absorptive dust. In the mid-visible band (497.5–692.5 nm), the single scattering albedos (SSAs) for the four dust size bins (0.1–1, 1–2, 2–3 and 3–6 µm) are 0.977, 0.943, 0.915 and 0.873 respectively. In the global mean, the bulk mid-visible SSA of dust (weighted by optical depth) is 0.961, confirming that dust is a weakly absorbing aerosol in our model. Due to the variation of SSA with particle radius, SSA tends to be somewhat smaller over major dust source regions (~0.95) and somewhat larger over remote regions (~0.97), as in Miller et al. (2004) .

ACPD
11, 1595–1639, 2011

Longwave effects of dust were included by tabulating single-scattering properties from OPAC (Optical Properties of Aerosols and Clouds; Hess et al., 1998), using their mineral dust nucleation and accumulation modes to represent the radiation scheme's small and large dust modes respectively.

2.2 Simulations

We compare two 160-year coupled atmosphere-ocean simulations with the CSIRO Mk3.6 GCM. Both simulations have forcing (greenhouse gases, anthropogenic aerosols and ozone) appropriate for the year 2000. The DUST run is a continuation of the 70-year run described by Rotstayn et al. (2010): we extended this run to a total of 240 years. The setup of the NODUST run is identical to that of the DUST run, except that the Australian dust source is set to zero. NODUST was initialised from the end of the above 70-year run, and was also integrated to the end of year 240. We show results from the last 160 years of both simulations, to allow for a 10-year spinup period in NODUST. Hereafter, we label these as years 1 to 160, so that year 1 is equivalent to year 81 in the original terminology. To investigate dust-ENSO interactions, we will mainly focus on the Austral spring season, September to November (SON), when the effect of ENSO on Australian rainfall is strongest (McBride and Nicholls, 1983).

The simulation of mean seasonal Australian climate in the earlier 70-year run was evaluated by Rotstayn et al. (2010), who found that in most respects the model performed well. In particular, calculation of a non-dimensional skill score (the "M-statistic"; Watterson, 1996), using data from all four seasons, confirmed that Mk3.6 gave a better simulation than a majority of GCMs from the Coupled Model Intercomparison Project Phase 3 (CMIP3).

ACPD
11, 1595–1639, 2011

3 Results and discussion

3.1 Dust simulation

The annual-mean global dust load from the DUST run is shown in Fig. 1. In common with other global modelling studies (e.g., Ginoux et al., 2001; Woodward, 2001; Tegen et al., 2002; Zender et al., 2003; Miller et al., 2006; Tanaka and Chiba, 2006; Yoshioka et al., 2007), the dominance of the sources in the Northern Hemisphere is obvious. The total global dust load is 35 Tg, towards the high end of the range (8–36 Tg) found in 16 global models reviewed by Zender et al. (2004). This is likely due to the treatment of sub-grid wind fluctuations in the dust emission scheme (Eq. 3), which contributes to a relatively large global dust emission (3569 Tg yr^{-1}) in the DUST run. This is somewhat larger than the range of 1000 to 3000 Tg that was found to be consistent with observations by Cakmur et al. (2006).

Figure 2 shows the direct radiative forcing of dust at the top of the atmosphere and the surface. We calculated these quantities by repeating the last 60 years of the DUST run with the inclusion of an additional radiation call every three hours (which is the usual interval between radiation calls in the model). The global-mean top-of-atmosphere direct radiative effect of dust in the DUST run is $-0.82\,W\,m^{-2}$ (shortwave) and $+0.26\,W\,m^{-2}$ (longwave). These values are similar to those obtained in two recent modelling studies that also used updated refractive indices to represent less absorptive dust particles than previously assumed: Miller et al. (2006) obtained $-0.62\,W\,m^{-2}$ (shortwave) and $+0.23\,W\,m^{-2}$ (longwave), and Yoshioka et al. (2007) obtained $-0.92\,W\,m^{-2}$ (shortwave) and $+0.32\,W\,m^{-2}$ (longwave). Due to the relatively high SSA (∼0.96) of dust, the top-of-atmosphere shortwave forcing is negative everywhere, unlike some other models, where more absorptive dust can give positive shortwave forcing over surfaces with high albedo. As in other models, surface shortwave forcing ($-2.19\,W\,m^{-2}$) is negative and surface longwave forcing ($+0.91\,W\,m^{-2}$) is positive. Over the major dust sources, longwave forcing can be comparable in magnitude to shortwave forcing, but it falls away more quickly with distance, since longwave

ACPD
11, 1595–1639, 2011

forcing has a larger relative contribution from large particles. Also, dust shortwave forcing over oceans is enhanced in relative terms by the lower surface albedo. A useful recent summary of results from other models is given by Yue et al. (2010); this shows that the surface radiative forcing in our model is within the range of other results. The magnitude of both our shortwave and longwave surface forcing is larger than average, probably due to our relatively large dust burden.

Before attempting to draw conclusions about the effects of dust in the Mk3.6 simulations, it is useful to compare the simulated distribution of Australian dust with observed values. Our observed distribution is based on a spatial pattern derived from Advanced Along-Track Scanning Radiometer (AATSR) satellite retrievals for the period 2002–2008. A new algorithm for aerosol retrieval from AATSR has been developed, which enables the retrieval of aerosol optical depth (AOD) and identification of aerosol types. The algorithm will be discussed in two separate papers that are currently in preparation. It is based on classification of local aerosol types reported by Qin and Mitchell (2009), using a clustering analysis of sunphotometer observations at CSIRO Aerosol Ground Station Network (AGSNet) sites, which are affiliated with NASA's Aerosol Robotic Network (Mitchell and Campbell, 2004). Among the Australian aerosol classes is a dust aerosol, the particle size distribution of which allows dust mass loading to be derived from the AATSR AOD.

Figure 3 shows observed and modelled dust loading over Australia for annual-mean and SON conditions. The model is broadly successful at capturing the spatial pattern of Australian dust, with the Lake Eyre Basin in central-eastern Australia as the dominant dust source. There is some evidence of a high bias in the modelled results relative to the satellite retrievals, especially in SON. The noisier pattern in the satellite-retrieved values probably reflects, at least in part, the much shorter time period for the satellite record (six years as opposed to 160 years in the model).

We have also compared the annual cycle of simulated aerosol optical depth with sunphotometer measurements from Tinga Tingana, a dust-dominated site in the Strzelecki Desert of South Australia (approximately 140° E, 29° S), which forms part of AGSNet.

ACPD
11, 1595–1639, 2011

A 10-year aerosol climatology at this site (Mitchell et al., 2010) showed dual peaks in AOD in September and January, the former including a significant fine-particle mode characteristic of smoke from long-range transport, while the January peak was dominated by coarse particles characteristic of wind-blown dust.

Figure 4 compares the observed and modelled annual cycles of AOD. The observational cycle is the AOD from Mitchell et al. (2010) interpolated to 530 nm, with vertical bars equal to one standard deviation. The modelled cycles show the seasonal variation of mid-visible AOD, both "total" and "dust only". The comparison suggests that the modelled total AOD is unrealistically high throughout the year, particularly during the spring and summer peaks. These peaks are not present in the model's "dust only" AOD, and are likely due to an excessive contribution to AOD from biomass burning in the model. This is especially true in January, when the biomass-burning emissions used in this version of the model are too large over eastern Australia; the emissions are based on satellite retrievals for the year 2000 (Ito and Penner, 2004, 2005), which are probably not representative of the long-term average. Plots of the modelled distribution of carbonaceous aerosol (not shown) indicate that the modelled AOD at Tinga Tingana is elevated by biomass-burning aerosol advected from northern Australia during the months of August to November, with a maximum effect in September. According to Mitchell et al. (2010), the observed AOD in September is also elevated by smoke aerosol from long-range transport, suggesting that this feature in the model is qualitatively realistic, though overestimated in magnitude.

In summary, the model qualitatively captures the annual cycle of AOD at Tinga Tingana, but overestimates the magnitude of the peaks in September and January due to an excessive contribution from biomass burning. Combining the results of Figs. 3 and 4, the model appears to moderately overestimate the Australian dust load and optical depth during the spring (SON) season, which will be the main focus of our study. This also seems consistent with our relatively large global dust load, and may be due to our treatment of sub-grid wind fluctuations in the dust emission scheme (Eq. 3).

ACPD
11, 1595–1639, 2011

3.2 Simulation of mean Australian climate

The simulation of seasonal-mean rainfall, surface air temperature and mean sea-level pressure (MSLP) in a shorter version of the DUST run was evaluated in detail by Rotstayn et al. (2010), who found an overall improvement relative to earlier versions of the model. Before we investigated the ENSO-related rainfall variability in the DUST and NODUST simulations, we considered whether there were any significant effects of Australian dust on the simulation of mean Australian climate by Mk3.6. When we compared the DUST and NODUST runs, we found that differences in simulated mean rainfall and MSLP were generally small and insignificant.

Since we will focus on variability of rainfall during SON, we show the mean SON rainfall from observations and the model in Fig. 5. The DUST run (middle panel) is broadly able to capture the observed climatology shown in the left panel, although the model has a dry bias compared to the observations. The difference between the DUST and NODUST runs (right panel) confirms that, although there is an area in eastern Australia where the DUST run has slightly higher rainfall in SON, the differences are generally not statistically significant. This was also the case in other seasons (not shown).

However, there was a small but statistically significant increase of annual-mean surface air temperature over the Australian continent in the DUST run. This was seen more strongly in the daily minimum temperatures (0.24 K) than in daily maxima (+0.09 K), corresponding to a decrease in the diurnal temperature range. A reduction of the diurnal temperature range has been noted before, both in observations (Washington et al., 2006) and a global model (Yue et al., 2010), but we do not consider it further in the present paper.

ACPD
11, 1595–1639, 2011

3.3 Observed and modelled ENSO-rainfall relationships

In this section, we will compare the ENSO-rainfall relationships in the DUST and NODUST runs with corresponding observed relationships during SON, using standard linear regression. Sea surface temperature (SST) observations are the 1° gridded analysis from HadISST2 (Rayner et al., 2003), and rainfall observations are from the Australian Water Availability Project (AWAP; Jones et al., 2009). We follow the common practice of measuring the state of ENSO using SST averaged over the Niño 3.4 region (170° W–120° W, 5° S–5° N). The standard deviation of Niño 3.4 SST (taking each SON average as a single data point) is 0.64 K in DUST and 0.63 K in NODUST (compared to 0.81 K in HadISST2). Thus, when we show the results of the linear regression relative to a 1 K change in Niño 3.4 SST, this represents somewhat less than a ±1 standard deviation change.

Figure 6 shows the observed relationships between Niño3.4 SST and Australian rainfall for the period 1901–2007. These plots confirm the results of earlier studies, that there is a strong relationship between ENSO and Australian rainfall in spring, mainly over the eastern two-thirds of the continent (McBride and Nicholls, 1983; Ropelewski and Halpert, 1987).

Figure 7 shows the same relationships for the DUST run. The model is rather successful at capturing the observed relationships, with significant correlations between −0.25 and −0.55 over most of eastern Australia, and regression slopes that are comparable in magnitude to those in the right panel of Fig. 6. Note that, due to the model's relatively coarse resolution (approximately 1.9°, compared to 0.25° in the observations), it would not be expected to resolve the enhanced rainfall over the Alps in south-eastern Australia, or along the Queensland coast. Over some parts of central-eastern Australia, the modelled correlations and regression slopes are somewhat stronger than the observed values.

In the NODUST run (Fig. 8), the ENSO-rainfall relationships are markedly weaker, and they tend to agree less well with the observed relationships. Over substantial

ACPD
11, 1595–1639, 2011

areas of eastern Australia, the correlations are not significant ($|r| < 0.25$). The region of significant correlation also extends further to the west in NODUST, which agrees less well with the observed relationship.

Figure 9 shows the difference of the Niño3.4 SST – rainfall regression slopes between the DUST and NODUST runs. Statistical significance is assessed using a t-test for the difference of regression slopes (Zar, 1996, chapter 17). This plot confirms that inclusion of Australian dust amplifies the modelled ENSO-rainfall relationship over eastern Australia and weakens it over parts of western Australia. In total, there are 19 grid points over eastern Australia (stippled in the plot) where the Niño3.4 SST – rainfall regression slope is significantly different in the two runs.

Is the stronger ENSO-rainfall relationship over eastern Australia in the DUST run due to wet years becoming wetter, dry years becoming drier, or both? For each of the SON seasons, we averaged the rainfall over the stippled points in eastern Australia in Fig. 9, and plotted a scatter diagram of these 160 data points against Niño3.4 SST for both runs (not shown). This confirmed the above result that the regression slope is steeper in DUST than in NODUST, and the correlation between Niño3.4 SST and rainfall is also markedly stronger in DUST ($r = -0.48$) than in NODUST ($r = -0.27$). To make this clearer, we sorted the data points into 0.5° Niño3.4-SST bins, and plotted them as a histogram in Fig. 10. This confirms that wet years are wetter and dry years are drier in the DUST run (red bars) than in the NODUST run (blue bars). There is a monotonic change in the effect of dust with increasing SST: there is a dust-induced rainfall increase of 39%, 28% and 18% in the first, second and third SST bins, and a dust-induced rainfall decrease of 2.5% and 17% in the fourth and fifth SST bins. This also shows that, even in relative terms, the effect of dust is stronger in wet years than in dry years. It is also seen that, averaged over the points used to construct the histogram, the DUST run has slightly higher rainfall in SON than the NODUST run; this is consistent with the small (and non-significant) change in mean SON rainfall shown in Fig. 5c.

ACPD
11, 1595–1639, 2011

3.4 Possible mechanism of dust-ENSO feedback

Is the dust radiative forcing over Australia large enough to exert substantial dynamic effects? In Fig. 11 we show average dust shortwave atmospheric heating and surface radiative forcing for SON, averaged over the latitude range 20.5° S to 29.8° S. The latitude range was chosen to roughly capture the region where the dust-induced change in the regression slope of rainfall versus Niño3.4-SST is significant in Fig. 9, and end points of the range correspond to the edges of model grid boxes. Peak atmospheric heating of more than 0.1 K day^{-1} occurs near the surface at about 130° E. Somewhat larger values were shown for SON over Australia by Miller et al. (2004), but their mid-visible SSA was substantially lower (0.906 in the global mean, compared to 0.961 in our model), so this seems fairly consistent. Comparison with other studies suggests that these heating rates are large enough to induce significant circulation changes. For example, Lau et al. (2006) simulated aerosol shortwave heating rates of 0.2 to 0.4 K day^{-1} over the Tibetan Plateau, and argued that the convection induced by this "elevated heat pump" draws in warm and moist air over the Indian subcontinent prior to the onset of the monsoon. Dust surface radiative forcing in our simulation is also substantial: it reaches almost −10 W m^{-2} near 137° E, and its magnitude exceeds 4 W m^{-2} over a wide area.

Rotstayn et al. (2010) showed that dust loading over Australia in Mk3.6 is strongly correlated with ENSO, especially over eastern and northern Australia. This makes sense, because rainfall strongly affects the source function for dust (via its effect on soil moisture) as well as the sink via wet deposition. We thus expect that dust radiative forcing will also be correlated with ENSO in the DUST run.

To examine the dust-ENSO dynamic feedback in more detail, we regressed three-dimensional dust concentrations and dust shortwave heating rates against Niño3.4-SST, and averaged the regression slopes over the latitude range 20.5° S to 29.8° S. The regression of dust concentration against Niño3.4-SST is shown in Fig. 12. East of about 125° E, dust concentration increases with Niño3.4-SST, with the strongest

ACPD
11, 1595–1639, 2011

response centred below 900 hPa and between about 135° E and 150° E. The location of the positive correlation is consistent with the area where SON rainfall is positively correlated with Niño3.4-SST in Fig. 7, and also agrees quite well with the area in eastern Australia where the dust-induced enhancement of the rainfall–ENSO relationship is significant (Fig. 9). There is a smaller area west of about 125° E where dust concentration decreases with Niño3.4-SST, although this relationship is less strong than the increase over eastern Australia. This decrease cannot be explained by changes in rainfall, and is due to a decrease of surface wind speed with Niño3.4-SST in that region (Fig. 13). This is part of a larger pattern that extends westward across the Indian Ocean, where the climatological easterly winds are weakend by enhanced westerly flow in El Niño years (not shown). This is consistent with a previously reported contraction and strengthening of the Hadley cell under El Niño (Lu et al., 2008), which increases confidence that it is associated with a coherent dynamical response.

How do the ENSO-induced changes in dust affect atmospheric heating and dust-induced radiative forcing at the surface? The regression of dust shortwave radiative forcing against Niño3.4-SST is shown in Fig. 14. East of about 120° E, increasing Niño3.4-SST gives an increase of dust-induced heating of the lower troposphere and cooling of the surface. The magnitude of the surface forcing peaks near 145° E, which is east of the maximum change in dust concentration, whereas the largest response of atmospheric heating is further to the west. The surface forcing is increased by lower surface albedo near the east coast, whereas atmospheric heating is increased by stronger insolation and higher surface albedo in the arid zone. West of about 120° E, there is a relatively small decrease of atmospheric heating with increasing Niño3.4-SST, related to the decrease of dust concentration shown in Fig. 12.

The water vapour balance of an atmospheric column in equilibrium is given by (Perlwitz and Miller, 2010)

$$-\nabla \cdot \boldsymbol{M}_q = P - E \tag{4}$$

where $\boldsymbol{M}_q$ is the horizontal flux of specific humidity integrated over the atmospheric column, E is evaporation of water vapour from the underlying surface, and P is

ACPD
11, 1595–1639, 2011

precipitation. Equation 4 can also be used to estimate the contribution to precipitation from moisture transport (derived as $P-E$), assuming no net accumulation of moisture in the column. Figure 15 shows $P-E$, sorted into 0.5° Niño3.4-SST bins, for the same model columns used in Fig. 10. This suggests that in the DUST run, precipitation in these columns is enhanced by moisture convergence in the first two SST bins, whereas in NODUST there is net atmospheric moisture divergence across all SST bins.

Numerous studies have shown that aerosols reduce surface insolation, which must be balanced by weaker latent and sensible heat fluxes (Ramanathan et al., 2001; Roderick and Farquhar, 2002; Liepert et al., 2004). Absorption of shortwave radiation by aerosols such as dust also causes heating of the lower troposphere and cooling of the surface, which is expected to stabilise the lower atmosphere and reduce convection (Satheesh and Moorthy, 2005). This has been shown on regional scales in several modelling studies (Jiang and Feingold, 2006; Grini et al., 2006; Fan et al., 2008; Wendisch et al., 2008). Our results suggest that under suppressed (El Niño) conditions, the surface radiative effect of dust reduces convection in this manner. However, there is also evidence that diabatic heating due to absorbing aerosols can enhance ascent and moisture convergence, leading to increased convection and precipitation (Stephens et al., 2004; Lau et al., 2006; Randles and Ramaswamy, 2008; Solmon et al., 2008; Lau et al., 2009; Perlwitz and Miller, 2010). In a recent attempt to synthesise the semi-direct effects of absorbing aerosols, Koch and Del Genio (2010) argued that absorbing aerosols below cloud may enhance convection and cloud cover. The climatological SON cloud cover over Australia in our model lies mostly above the dust layer (not shown). It is thus possible that this is the dominant mechanism in our model under convective (La Niña) conditions in eastern Australia.

Over parts of north-western Australia, dust concentration decreases with increasing Niño3.4-SST (due to a decrease of wind speed), and this may explain why the amplitude of the ENSO-related rainfall response is weakened there in the DUST run. The area of decreasing wind speed with increasing Niño3.4-SST agrees well with the stippled area in north-western Australia in Fig. 9. There may also be a compensating

ACPD
11, 1595–1639, 2011

circulation change over the north-west in response to the dust-induced changes over eastern Australia, along the lines of that described by Stephens et al. (2004).

3.5 Discussion of uncertainties

Our results show that, in the CSIRO Mk3.6 GCM, dust over eastern Australia tends to exert a negative feedback on rainfall under El Niño conditions and a positive feedback under La Niña conditions. This is intriguing, because it suggests that the radiative feedback of dust on rainfall is potentially of opposite sign under suppressed and convective conditions. We noted examples in the literature of negative and positive feedbacks on convection due to the radiative effects of absorbing aerosols. However, further work is needed to understand why a negative (positive) feedback should be dominant under suppressed (convective) conditions.

An interesting comparison is with Heinold et al. (2008), who described both positive and negative dust radiative feedbacks on surface wind speeds in a regional modelling study of Saharan dust over a one-week period. Dust feedbacks caused higher surface wind speeds when momentum was mixed downwards to the ground by turbulence. Under stable conditions, thermal stratification suppressed turbulent mixing and dust-induced stabilisation caused lower surface wind speeds. Although the context is slightly different, their study provides a precedent whereby dust can generate positive and negative feedbacks, depending on the atmospheric stratification and the degree of stabilisation by mineral dust.

The preceding arguments are based on the shortwave radiative effects of dust. Our model does include longwave effects of dust, and a number of studies confirm that these are non-negligible (e.g., Highwood et al., 2003; Haywood et al., 2005; Hansell et al., 2010; Yue et al., 2010). We justify this simplification because convective rainfall over continental areas in GCMs is usually largest in the middle of the day, when dust shortwave effects are likely to be much larger than longwave effects. During the day, solar heating over land increases the lower-tropospheric temperature (and moisture) and hence instability, leading to development of convection. In observations,

ACPD
11, 1595–1639, 2011

the resulting convective precipitation maximum tends to occur in the late afternoon or evening (Nesbitt and Zipser, 2003), whereas GCMs tend to lead the observed diurnal cycle by several hours (Yang and Slingo, 2001; Collier and Bowman, 2004). In our current simulations, we only saved monthly mean output, so we are unable to resolve the diurnal cycle, but this may be important for a more rigorous analysis.

In addition to the above analysis, we considered whether dust-induced changes in atmospheric circulation or evaporation of moisture from the ocean surface could explain the different rainfall response in the DUST and NODUST runs. However, we were unable to find a plausible explanation via these avenues. It is possible that diagnostics of moisture transport (which were not available to us) would yield valuable insight. Another possible approach is the use of composites, to separately examine warm and cool ENSO events.

Another uncertainty concerns the simulation of ENSO itself in the model. In common with most other GCMs, Mk3.6 suffers from the Pacific equatorial cold-tongue bias: the tongue of SST anomalies associated with ENSO extends too far west towards the eastern Indian Ocean, which is expected to generate an ENSO-rainfall relationship that is centred too far west over Australia (e.g., Shi et al., 2008). This suggests that a useful extension of the present study would be to perform an ensemble of atmosphere-only runs following the protocol of the Atmospheric Model Intercomparison Project (AMIP). However, it should be noted that such atmosphere-only simulations also have limitations, e.g., inclusion of a radiative perturbation may alter the land-sea contrast in an unrealistic way, since SSTs are unable to respond to the perturbation.

Comparison with observations suggests that the radiative effects of dust may be over-estimated in our model, so the impact of dust on the simulated rainfall variability may also be exaggerated. On the other hand, the model uses prescribed vegetation, so possible feedbacks due to interannual and interdecadal changes in vegetation properties are not simulated. In principle, these might be expected to enhance the variability of the dust source in response to natural rainfall fluctuations.

ACPD
11, 1595–1639, 2011

4 Summary and conclusions

We compared two 160-year coupled atmosphere-ocean simulations of modern-day climate using the CSIRO Mk3.6 GCM. The DUST simulation included an interactive treatment of mineral dust and its direct radiative effects. This was a longer version of a similar run described by Rotstayn et al. (2010), who noted an improved simulation of Australian rainfall variability in Mk3.6 compared to its predecessor (Mk3.5) and several other GCMs. They hypothesised that "active" dust (which interacts with the model's hydrological cycle) might contribute to the improved simulation in Mk3.6 relative to Mk3.5. Their hypothesis was based on qualitative arguments, since they did not have access to a pair of simulations in which only one thing was changed. This motivated us to perform a second run (NODUST), which was identical to DUST, except that the Australian dust source was set to zero.

Comparison of the dust simulation with observations and other models led us to conclude that our dust concentrations and resultant radiative forcing are probably somewhat too large. We attributed this to the treatment of sub-grid wind speed used in the dust emission scheme. However, the spatial pattern of dust over Australia was captured rather well by our model, in which the dust emission scheme assigns enhanced erodibility to topographic depressions (Ginoux et al., 2001).

To investigate possible dust-ENSO-rainfall feedbacks in the model, we focused on the austral spring season (SON), when the correlation between rainfall and ENSO is strongest over Australia. We used ordinary least squares linear regression against Niño3.4-SST to characterise the variation of rainfall, dust and other quantities with respect to ENSO. We found that the ENSO-rainfall relationship over eastern Australia was stronger in the DUST run: dry (El Niño) years tended to be drier, and wet (La Niña) years wetter. The ENSO-rainfall relationship was also weaker over north-western Australia in the DUST run. The amplification of ENSO-related rainfall variability over eastern Australia and the weaker ENSO-rainfall relationship over the north-west both represented an improvement relative to observations. Over eastern Australia, dust

ACPD
11, 1595–1639, 2011

loading showed a positive relationship with Niño3.4-SST, due to the strong negative dependence of dust concentration on rainfall in the model. The proposed mechanism over eastern Australia involved stabilisation of the surface layer due to enhanced shortwave atmospheric heating and surface cooling in El Niño years, and enhanced ascent and moisture convergence driven by dust-induced radiative heating in La Niña years. Over parts of north-western Australia, dust loading showed a negative relationship with Niño3.4-SST, which was explained by decreasing near-surface wind speeds with increasing Niño3.4-SST. The location of these decreasing wind speeds agreed well with the region where the dust-ENSO relationship was significantly weakened by inclusion of dust. It thus seems plausible that, in that region, inclusion of dust acts to weaken the ENSO-rainfall relationship via an inverse process to that which occurs over eastern Australia. As discussed in Sect. 3.5, these arguments are only tentative at present, and further work is needed to clarify the mechanism.

Although the Australian dust source is smaller than the major sources in the Northern Hemisphere, our results show that the direct radiative effects of Australian dust may have important interactions with climate variability. The results suggest that (1) a realistic treatment of Australian dust may be necessary for accurate simulation of the ENSO-rainfall relationship over Australia, and (2) radiative feedbacks involving dust may be important for understanding natural rainfall variability over Australia. (1) is potentially important for climate modelling, because ENSO dominates rainfall variability over most of eastern and central Australia, and the response of ENSO to climate change is an active research question (Collins et al., 2010). (2) raises various research questions, e.g., it is possible that there is a positive feedback on drought induced by the recent observed increase in Australian dust (Mitchell et al., 2010). Although our model tends to over-estimate the Australian dust source, it is possible that the use of prescribed vegetation causes rainfall-dust feedbacks to be under-estimated in some respects. It would be intriguing to explore these effects using a model that includes dynamic vegetation in a future study.

ACPD
11, 1595–1639, 2011

Acknowledgements. This work was funded in part by the Australian Climate Change Science Program (ACCSP).

References

Bullard, J., Baddock, M., McTainsh, G., and Leys, J.: Sub-basin scale dust source geomorphology detected using MODIS, Geophys. Res. Lett., 35, L15404, doi:10.1029/2008GL033928, 2008. 1598

Cakmur, R. V., Miller, R. L., Perlwitz, J., Geogdzhayev, I. V., Ginoux, P., Koch, D., Kohfeld, K. E., Tegen, I., and Zender, C. S.: Constraining the magnitude of the global dust cycle by minimizing the difference between a model and observations, J. Geophys. Res., 111, D6207, doi:10.1029/2005JD005791, 2006. 1604

Chou, M.-D. and Lee, K.-T.: A Parameterization of the Effective Layer Emission for Infrared Radiation Calculations, J. Atmos. Sci., 62, 531–541, 2005. 1600

Collier, J. C. and Bowman, K. P.: Diurnal cycle of tropical precipitation in a general circulation model, J. Geophys. Res., 109, D17105, doi:10.1029/2004JD004818, 2004. 1614

Collins, M., An, S.-I., Cai, W., Ganachaud, A., Guilyardi, E., Jin, F.-F., Jochum, M., Lengaigne, M., Power, S., Timmermann, A., Vecchi, G., and Wittenberg, A.: The impact of global warming on the tropical Pacific ocean and El Nino, Nat. Geosci., 3, 391–397, doi:10.1038/NGEO868, 2010. 1616

Cook, B. I., Miller, R. L., and Seager, R.: Amplification of the North American "Dust Bowl" drought through human-induced land degradation, P. Natl. Acad. Sci. USA, 106, 4997–5001, doi:10.1073/pnas.0810200106, 2009. 1598

Deardorff, J. W.: Convective velocity and temperature scales for the unstable planetary boundary layer and for Rayleigh convection, J. Atmos. Sci., 27, 1211–1213, 1970. 1601

Dubovik, O., Holben, B., Eck, T., Smirnov, A., Kaufman, Y., King, M., Tanre, D., and Slutsker, I.: Variability of absorption and optical properties of key aerosol types observed in worldwide locations, J. Atmos. Sci., 59, 590–608, 2002. 1602

Evan, A. T., Dunion, J., Foley, J. A., Heidinger, A. K., and Velden, C. S.: New evidence for a relationship between Atlantic tropical cyclone activity and African dust outbreaks, Geophys. Res. Lett., 33, L19813, doi:10.1029/2006GL026408, 2006. 1598

Fan, J., Zhang, R., Tao, W., and Mohr, K. I.: Effects of aerosol optical properties on

ACPD

11, 1595–1639, 2011

deep convective clouds and radiative forcing, J. Geophys. Res., 113, D8209, doi:10.1029/2007JD009257, 2008. 1612
Fécan, F., Marticorena, B., and Bergametti, G.: Parametrization of the Increase of the Aeolian Erosion Threshold Wind Friction Velocity Due to Soil Moisture for Arid and Semi-Arid Areas, Ann. Geophysicae., 17, 149–157, 1999. 1597
Gillette, D. A. and Passi, R.: Modeling dust emission caused by wind erosion, J. Geophys. Res., 93, 14233–14242, 1988. 1597
Ginoux, P., Chin, M., Tegen, I., Prospero, J. M., Holben, B., Dubovik, O., and Lin, S.-J.: Sources and distributions of dust aerosols simulated with the GOCART model, J. Geophys. Res., 106, 20255–20273, doi:10.1029/2000JD000053, 2001. 1600, 1601, 1602, 1604, 1615
Ginoux, P., Prospero, J. M., Torres, O., and Chin, M.: Long-term simulation of global dust distribution with the GOCART model: correlation with North Atlantic Oscillation, Environ. Modell. Softw., 19, 113–128, 2004. 1600, 1601
Gordon, H. B., O'Farrell, S. P., Collier, M. A., Dix, M. R., Rotstayn, L. D., Kowalczyk, E. A., Hirst, A. C., and Watterson, I. G.: The CSIRO Mk3.5 Climate Model, Technical Report No. 21, The Centre for Australian Weather and Climate Research, Aspendale, Vic., Australia, 62 pp., available online at: http://www.cawcr.gov.au/publications/technicalreports.php, 2010. 1600
Grant, K. E., Chuang, C. C., Grossman, A. S., and Penner, J. E.: Modeling the spectral optical properties of ammonium sulfate and biomass burning aerosols: parameterization of relative humidity effects and model results, Atmos. Environ., 33, 2603–2620, 1999. 1600
Gregory, D. and Rowntree, P. R.: A mass flux convection scheme with representation of cloud ensemble characteristics and stability-dependent closure, Mon. Weather Rev., 118, 1483–1506, 1990. 1602
Grini, A., Tulet, P., and Gomes, L.: Dusty weather forecasts using the MesoNH mesoscale atmospheric model, J. Geophys. Res., D19205, doi:10.1029/2005JD007007, 2006. 1612
Hansell, R. A., Tsay, S. C., Ji, Q., Hsu, N. C., Jeong, M. J., Wang, S. H., Reid, J. S., Liou, K. N., and Ou, S. C.: An Assessment of the Surface Longwave Direct Radiative Effect of Airborne Saharan Dust during the NAMMA Field Campaign, J. Atmos. Sci., 67, 1048–1065, doi:10.1175/2009JAS3257.1, 2010. 1613
Haywood, J., Francis, P., Osborne, S., Glew, M., Loeb, N., Highwood, E., Tanré, D., Myhre, G., Formenti, P., and Hirst, E.: Radiative properties and direct radiative effect of Saharan dust measured by the C-130 aircraft during SHADE: 1. Solar spectrum, J. Geophys. Res., 108, 8577, doi:10.1029/2002JD002687, 2003. 1597

ACPD
11, 1595–1639, 2011

Haywood, J. M., Allan, R. P., Culverwell, I., Slingo, T., Milton, S., Edwards, J., and Clerbaux, N.: Can desert dust explain the outgoing longwave radiation anomaly over the Sahara during July 2003?, J. Geophys. Res., 110, D05105, doi:10.1029/2004JD005232, 2005. 1613

Heinold, B., Tegen, I., Schepanski, K., and Hellmuth, O.: Dust radiative feedback on Saharan boundary layer dynamics and dust mobilization, Geophys. Res. Lett., 35, L20817, doi:10.1029/2008GL035319, 2008. 1613

Hess, M., Koepke, P., and Schult, I.: Optical properties of aerosols and clouds: The software package OPAC, B. Ame. Meteor. Soc., 79, 831–844, 1998. 1603

Highwood, E. J., Haywood, J. M., Silverstone, M. D., Newman, S. M., and Taylor, J. P.: Radiative properties and direct effect of Saharan dust measured by the C-130 aircraft during Saharan Dust Experiment (SHADE): 2. Terrestrial spectrum, J. Geophys. Res., 108, 8578, doi:10.1029/2002JD002552, 2003. 1613

Holtslag, A. A. M. and Boville, B. A.: Local versus non-local boundary layer diffusion in a global climate model, J. Climate, 6, 1825–1842, 1993. 1602

Ishizuka, M., Mikami, M., Leys, J., Yamada, Y., Heidenreich, S., Shao, Y., and McTainsh, G. H.: Effects of soil moisture and dried raindroplet crust on saltation and dust emission, J. Geophys. Res., 113, D24212, doi:10.1029/2008JD009955, 2008. 1597

Ito, A. and Penner, J. E.: Global estimates of biomass burning emissions based on satellite imagery for the year 2000, J. Geophys. Res., 109, D14S05, doi:10.1029/2003JD004423, 2004. 1606

Ito, A. and Penner, J. E.: Historical emissions of carbonaceous aerosols from biomass and fossil fuel burning for the period 1870–2000, Glob. Biogeochem. Cy., 19, GB2028, doi:10.1029/2004GB002374, 2005. 1606

Jiang, H. and Feingold, G.: Effect of aerosol on warm convective clouds: Aerosol-cloud-surface flux feedbacks in a new coupled large eddy model, J. Geophys. Res., 111, D01202, doi:10.1029/2005JD006138, 2006. 1612

Jones, D. A., Wang, W., and Fawcett, R.: High-quality spatial climate data-sets for Australia, Aust. Meteorol. Oceanogr. J., 58, 233–248, 2009. 1608

Koch, D. and Del Genio, A. D.: Black carbon semi-direct effects on cloud cover: review and synthesis, Atmos. Chem. Phys., 10, 7685–7696, doi:10.5194/acp-10-7685-2010, 2010. 1612

Lau, K. M., Kim, M. K., and Kim, K. M.: Asian summer monsoon anomalies induced by aerosol direct forcing: the role of the Tibetan Plateau, Clim. Dynam., 26, 855–864, doi:10.1007/s00382-006-0114-z, 2006. 1610, 1612

ACPD
11, 1595–1639, 2011

Lau, K. M., Kim, K. M., Sud, Y. C., and Walker, G. K.: A GCM study of the response of the atmospheric water cycle of West Africa and the Atlantic to Saharan dust radiative forcing, Ann. Geophys., 27, 4023–4037, doi:10.5194/angeo-27-4023-2009, 2009. 1612
Liao, H. and Seinfeld, J. H.: Effect of clouds on direct aerosol radiative forcing of climate, J. Geophys. Res., 103, 3781–3788, 1998. 1597
Liepert, B. G., Feichter, J., Lohmann, U., and Roeckner, E.: Can aerosols spin down the water cycle in a warmer and moister world?, Geophys. Res. Lett., 31, L06207, doi:10.1029/2003GL019060, 2004. 1612
Louis, J.-F.: A Parametric Model of Vertical Eddy Fluxes in the Atmosphere, Bound. Layer Meteorol., 17, 187–202, 1979. 1602
Lu, J., Chen, G., and Frierson, D. M. W.: Response of the Zonal Mean Atmospheric Circulation to El Nino versus Global Warming, J. Climate, 21, 5835–5851, doi:10.1175/2008JCLI2200.1, 2008. 1611
Lunt, D. J. and Valdes, P. J.: The modern dust cycle: Comparison of model results with observations and study of sensitivities, J. Geophys. Res., 107, 4669, doi:10.1029/2002JD002316, 2002. 1601
Mackie, D. S., Boyd, P. W., McTainsh, G. H., Tindale, N. W., Westberry, T. K., and Hunter, K. A.: Biogeochemistry of iron in Australian dust: From eolian uplift to marine uptake, Geochem. Geophys. Geosyst., 9, Q03Q08, doi:10.1029/2007GC001813, 2008. 1597, 1598
McBride, J. L. and Nicholls, N.: Seasonal relationships between Australian rainfall and the Southern Oscillation, Mon. Weather Rev., 111, 1998–2004, 1983. 1603, 1608
McGregor, J. L.: Economical Determination of Departure Points for Semi-Lagrangian Models, Mon. Weather Rev., 121, 221–230, 1993. 1602
McTainsh, G. H., Leys, J. F., and Nickling, W.: Wind erodibility of arid lands in the channel country of western Queensland, Australia, Z. Geomorphol., 116, 113–130, 1999. 1597
McTainsh, G. H., Tews, E. K., and Leys, J. F. Bastin, G.: Spatial and temporal trends in wind erosion of Australian rangelands during 1960 to 2005 using the Dust Storm Index (DSI), Report for the Australian Collaborative Rangeland Information System [ACRIS], available at: http://www.environment.gov.au/land/publications/acris/wind-erosion.html, 2007. 1598
Miller, R. L., Tegen, I., and Perlwitz, J.: Surface radiative forcing by soil dust aerosols and the hydrologic cycle, J. Geophys. Res., 109, D04203, doi:10.1029/2003JD004085, 2004. 1597, 1602, 1610
Miller, R. L., Cakmur, R. V., Perlwitz, J., Geogdzhayev, I. V., Ginoux, P., Koch, D., Kohfeld,

ACPD
11, 1595–1639, 2011

K. E., Prigent, C., Ruedy, R., Schmidt, G. A., and Tegen, I.: Mineral dust aerosols in the NASA goddard institute for Space Sciences ModelE atmospheric general circulation model, J. Geophys. Res., 111, D06208, doi:10.1029/2005JD005796, 2006. 1604

Mitchell, R. M. and Campbell, S. K.: The Australian Aerosol Ground Station Network: Status Report and Development of a Radiometric Calibration Facility, Optica Pura y Aplicada, 37, 3259–3262, 2004. 1605

Mitchell, R. M., Campbell, S. K., and Qin, Y.: Recent increase in aerosol loading over the Australian arid zone, Atmos. Chem. Phys., 10, 1689–1699, doi:10.5194/acp-10-1689-2010, 2010. 1598, 1599, 1606, 1616

Myhre, G., Grini, A., Haywood, J. M., Stordal, F., Chatenet, B., Tanré, D., Sundet, J. K., and Isaksen, I. S. A.: Modeling the radiative impact of mineral dust during the Saharan Dust Experiment (SHADE) campaign, J. Geophys. Res., 108, 8579, doi:10.1029/2002JD002566, 2003. 1602

Nesbitt, S. W. and Zipser, E. J.: The diurnal cycle of rainfall and convective intensity according to three years of TRMM measurements, J. Climate, 16, 1456–1475, 2003. 1614

Penner, J. E., Zhang, S. Y., and Chuang, C. C.: Soot and smoke aerosol may not warm climate, J. Geophys. Res., 108, 4657, doi:10.1029/2003JD003409, 2003. 1597

Perlwitz, J. and Miller, R. L.: Cloud cover increase with increasing aerosol absorptivity: A counterexample to the conventional semidirect aerosol effect, J. Geophys. Res., 115, D08203, doi:10.1029/2009JD012637, 2010. 1611, 1612

Prospero, J. M. and Lamb, P. J.: African Droughts and Dust Transport to the Caribbean: Climate Change Implications, Science, 302, 1024–1027, doi:10.1126/science.1089915, 2003. 1597

Prospero, J. M., Ginoux, P., Torres, O., Nicholson, S. E., and Gill, T. E.: Environmental characterization of global sources of atmospheric soil dust identified with the NIMBUS 7 Total Ozone Mapping Spectrometer (TOMS) absorbing aerosol product, Rev. Geophys., 40, 1002, doi:10.1029/2000RG000095, 2002. 1598, 1601

Qin, Y. and Mitchell, R. M.: Characterisation of episodic aerosol types over the Australian continent, Atmos. Chem. Phys., 9, 1943–1956, doi:10.5194/acp-9-1943-2009, 2009. 1605

Ramanathan, V., Crutzen, P. J., Kiehl, J. T., and Rosenfeld, D.: Aerosols, climate and the hydrological cycle, Science, 294, 2119–2124, 2001. 1612

Randles, C. A. and Ramaswamy, V.: Absorbing aerosols over Asia: A Geophysical Fluid Dynamics Laboratory general circulation model sensitivity study of model response to aerosol optical depth and aerosol absorption, J. Geophys. Res., 113, D21203, doi:10.1029/

ACPD
11, 1595–1639, 2011

2008JD010140, 2008. 1612
Rayner, N. A., Parker, D. E., Horton, E. B., Folland, C. K., Alexander, L. V., Rowell, D. P., Kent, E. C., and Kaplan, A.: Globally complete analyses of sea surface temperature, sea ice and night marine air temperature, J. Geophys. Res., 108, 4407, doi:10.1029/2002JD002670, 2003. 1608
Redelsperger, J.-L., Guichard, F., and Mondon, S.: A Parameterization of Mesoscale Enhancement of Surface Fluxes for Large-Scale Models, J. Climate, 13, 402–421, 2000. 1601
Ridgwell, A. J.: Dust in the Earth system: the biogeochemical linking of land, air and sea, Philos. Trans. R. Soc. Lond. Ser. A-Math. Phys. Eng. Sci., 360, 2905–2924, doi:10.1098/rsta.2002.1096, 2002. 1597
Roderick, M. L. and Farquhar, G. D.: The cause of decreased pan evaporation over the past 50 years, Science, 298, 1410–1411, 2002. 1612
Ropelewski, C. F. and Halpert, M. S.: Global and regional scale precipitation associated with El Niño/Southern Oscillation, Mon. Weather Rev., 115, 1606–1626, 1987. 1608
Rosenfeld, D., Rudich, Y., and Lahav, R.: Desert dust suppressing precipitation: a possible desertification feedback loop, Proc. Natl. Acad. Sci., 98, 5975–5980, 2001. 1597
Rotstayn, L. D. and Lohmann, U.: Simulation of the tropospheric sulfur cycle in a global model with a physically based cloud scheme, J. Geophys. Res., 107, 4592, doi:10.1029/2002JD002128, 2002. 1602
Rotstayn, L. D., Cai, W., Dix, M. R., Farquhar, G. D., Feng, Y., Ginoux, P., Herzog, M., Ito, A., Penner, J. E., Roderick, M. L., and Wang, M.: Have Australian Rainfall and Cloudiness Increased Due to the Remote Effects of Asian Anthropogenic Aerosols?, J. Geophys. Res., 112, D09202, doi:10.1029/2006JD007712, 2007. 1600
Rotstayn, L. D., Collier, M. A., Feng, Y., Gordon, H. B., O'Farrell, S. P., Smith, I. N., and Syktus, J.: Improved simulation of Australian climate and ENSO-related rainfall variability in a GCM with an interactive aerosol treatment, Int. J. Climatol., 30, 1067–1088, doi:10.1002/joc.1952, 2010. 1598, 1599, 1600, 1602, 1603, 1607, 1610, 1615
Satheesh, S. K. and Moorthy, K. K.: Radiative effects of natural aerosols: A review, Atmos. Environ., 39, 2089–2110, 2005. 1596, 1597, 1612
Sato, M., Hansen, J. E., McCormick, M. P., and Pollack, J. B.: Stratospheric aerosol optical depth, 1850–1990, J. Geophys. Res., 98, 22,987–22,994, 1993. 1600
Shi, G., Cai, W., Cowan, T., Ribbe, J., Rotstayn, L., and Dix, M.: Variability and trend of the northwest Western Australia Rainfall: observations and coupled climate modeling, J. Cli-

ACPD
11, 1595–1639, 2011

mate, 21, 2938–2959, 2008. 1614
Smith, I. N.: Global climate modelling within CSIRO: 1981 to 2006, Aust. Meteorol. Mag., 56, 153–166, 2007. 1600
Solmon, F., Mallet, M., Elguindi, N., Giorgi, F., Zakey, A., and Konaré, A.: Dust aerosol impact on regional precipitation over western Africa, mechanisms and sensitivity to absorption properties, Geophys. Res. Lett., 35, L24705, doi:10.1029/2008GL035900, 2008. 1612
Stephens, G. L., Wood, N. B., and Pakula, L. A.: On the radiative effects of dust on tropical convection, Geophys. Res. Lett., 31, L23112, doi:10.1029/2004GL021342, 2004. 1612, 1613
Sun, D., Lau, W. K. M., Kafatos, M., Boybeyi, Z., Leptoukh, G., Yang, C., and Yang, R.: Numerical Simulations of the Impacts of the Saharan Air Layer on Atlantic Tropical Cyclone Development, J. Climate, 22, doi:10.1175/2009JCLI2738.1, 2009. 1598
Tanaka, T. Y. and Chiba, M.: A numerical study of the contributions of dust source regions to the global dust budget, Glob. Planet. Change, 52, 88–104, doi:10.1016/j.gloplacha.2006.02.002, 2006. 1598, 1604
Tegen, I., Harrison, S. P., Kohfeld, K., Prentice, I. C., Coe, M., and Heimann, M.: Impact of vegetation and preferential source areas on global dust aerosol: Results from a model study, J. Geophys. Res., 107, 4576, doi:10.1029/2001JD000963, 2002. 1604
van den Dool, H. M., Saha, S., and Johansson, A.: Empirical orthogonal teleconnections, J. Climate, 13, 1421–1435, 2000. 1598
van Leer, B.: Towards the Ultimate Conservative Difference Scheme. V. A New Approach to Numerical Convection, J. Comp. Phys., 23, 276–299, 1977. 1602
Washington, R., Todd, M., Middleton, N. J., and Goudie, A. S.: Dust-storm source areas determined by the total ozone monitoring spectrometer and surface observations, Ann. Ass. Am. Geogr., 93, 297–313, 2003. 1598
Washington, R., Todd, M. C., Engelstaedter, S., Mbainayel, S., and Mitchell, F.: Dust and the low-level circulation over the Bodélé Depression, Chad: Observations from BoDEx 2005, J. Geophys. Res., 111, D3201, doi:10.1029/2005JD006502, 2006. 1607
Watterson, I. G.: Non-dimensional measures of climate model performance, Int. J. Climatol., 16, 379–391, 1996. 1603
Webb, N. P., McGowan, H. A., Phinn, S. R., and McTainsh, G. H.: AUSLEM (AUStralian Land Erodibility Model): A tool for identifying wind erosion hazard in Australia, Geomorphology, 78, 179–200, doi:10.1016/j.geomorph.2006.01.012, 2006. 1597

ACPD
11, 1595–1639, 2011

Wendisch, M., Hellmuth, O., Ansmann, A., Heintzenberg, J., Engelmann, R., Althausen, D., Eichler, H., Wueller, D., Hu, M., Zhang, Y., and Mao, J.: Radiative and dynamic effects of absorbing aerosol particles over the Pearl River Delta, China, Atmos. Environ., 42, 6405–6416, doi:10.1016/j.atmosenv.2008.02.033, 2008. 1612

Woodward, S.: Modeling the atmospheric life cycle and radiative impact of mineral dust in the Hadley Centre climate model, J. Geophys. Res., 106, 18,155–18,166, 2001. 1604

Wurzler, S., Reisin, T. G., and Levin, Z.: Modification of mineral dust particles by cloud processing and subsequent effects on drop size, J. Geophys. Res., 105, 4501–4512, 2000. 1597

Yang, G. and Slingo, J.: The Diurnal Cycle in the Tropics, Mon. Weather Rev., 129, 784–801, doi:10.1175/1520-0493(2001)129(0784:TDCITT)2.0.CO;2, 2001. 1614

Yoshioka, M., Mahowald, N. M., Conley, A. J., Collins, W. D., Fillmore, D. W., Zender, C. S., and Coleman, D. B.: Impact of Desert Dust Radiative Forcing on Sahel Precipitation: Relative Importance of Dust Compared to Sea Surface Temperature Variations, Vegetation Changes, and Greenhouse Gas Warming, J. Climate, 20, 1445–1467, doi:10.1175/JCLI4056.1, 2007. 1598, 1604

Yu, H., Dickinson, R. E., Chin, M., Kaufman, Y. J., Zhou, M., Zhou, L., Tian, Y., Dubovik, O., and Holben, B. N.: Direct radiative effect of aerosols as determined from a combination of MODIS retrievals and GOCART simulations, J. Geophys. Res., 109, D03206, doi:10.1029/2003JD003914, 2004. 1602

Yue, X., Wang, H., Liao, H., and Fan, K.: Simulation of dust aerosol radiative feedback using the GMOD: 2. Dust-climate interactions, J. Geophys. Res., 115, D4201, doi:10.1029/2009JD012063, 2010. 1605, 1607, 1613

Zar, J. H.: Biostatistical Analysis, 3rd Edition, Prentice Hall International, London, 929 pp., 1996. 1609

Zender, C. S. and Kwon, E. Y.: Regional contrasts in dust emission responses to climate, J. Geophys. Res., 110, D13201, doi:10.1029/2004JD005501, 2005. 1597

Zender, C. S., Newman, D., and Torres, O.: Spatial heterogeneity in aeolian erodibility: Uniform, topographic, geomorphic, and hydrologic hypotheses, J. Geophys. Res., 108, doi:10.1029/2002JD003039, 2003. 1601, 1604

Zender, C. S., Miller, R. L., and Tegen, I.: Quantifying mineral dust mass budgets: terminology, constraints, and current estimates, Eos, 85, 509–512, doi:10.1029/2004EO480002, 2004. 1604

ACPD
11, 1595–1639, 2011

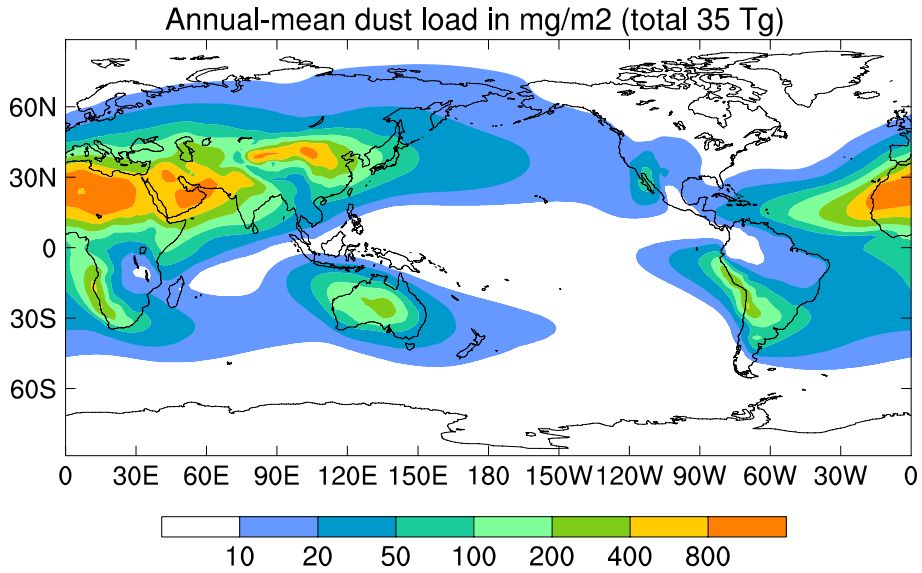

Fig. 1. Annual-mean simulated dust load in mg m^{-2}.

ACPD
11, 1595–1639, 2011

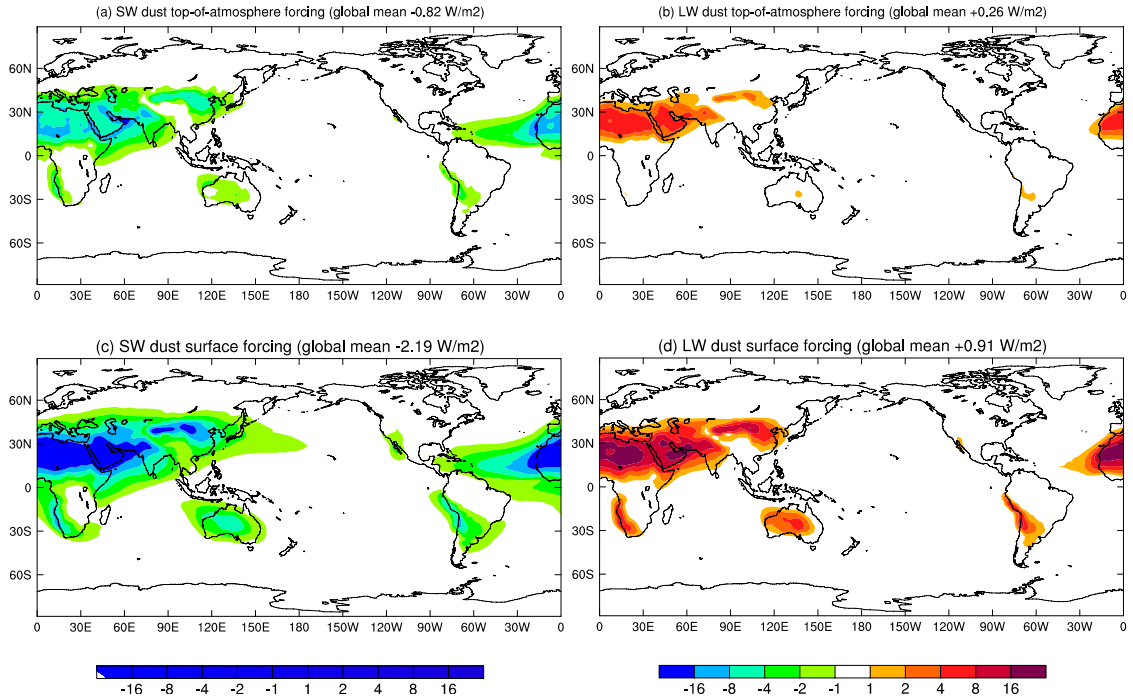

Fig. 2. Annual-mean simulated dust radiative forcing from the DUST run in W m^{-2} **(a)** shortwave at the top of the atmosphere, **(b)** longwave at the top of the atmosphere, **(c)** shortwave at the surface, and **(d)** longwave at the surface.

ACPD
11, 1595–1639, 2011

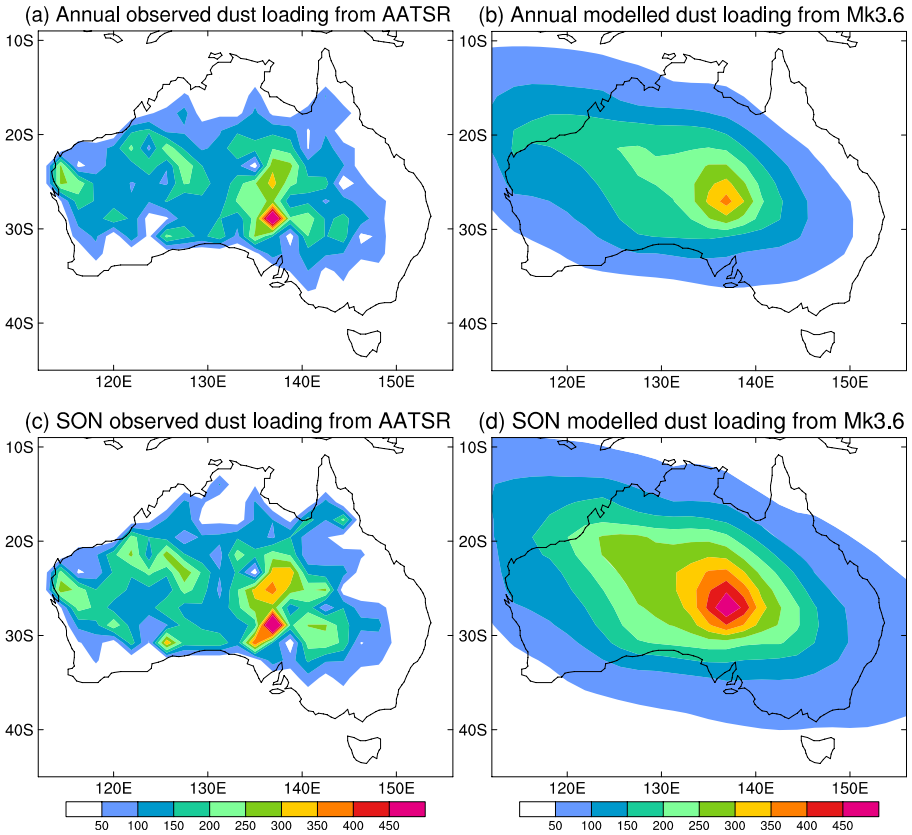

Fig. 3. Dust load over Australia **(a)** observed annual means, **(b)** simulated annual means, **(c)** observed for SON, **(d)** simulated for SON (in mg m^{-2}). Observations cover the period September 2002 to August 2007 for annual means, and September 2002 to November 2007 for SON.

ACPD
11, 1595–1639, 2011

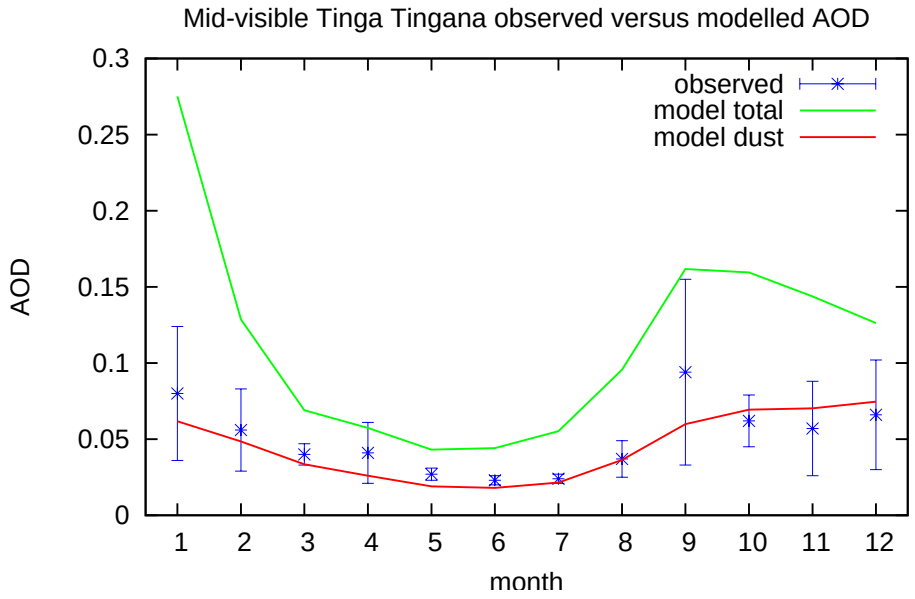

Fig. 4. Annual cycle of mid-visible aerosol optical depth at Tinga Tingana (approx. 140° E, 29° S). Sun photometer-based observed monthly means are shown in blue, with error bars denoting the standard deviation of individual observations. Modelled optical depths due to dust (red curve) and all tropospheric aerosols (green curve) are taken from the DUST run.

ACPD
11, 1595–1639, 2011

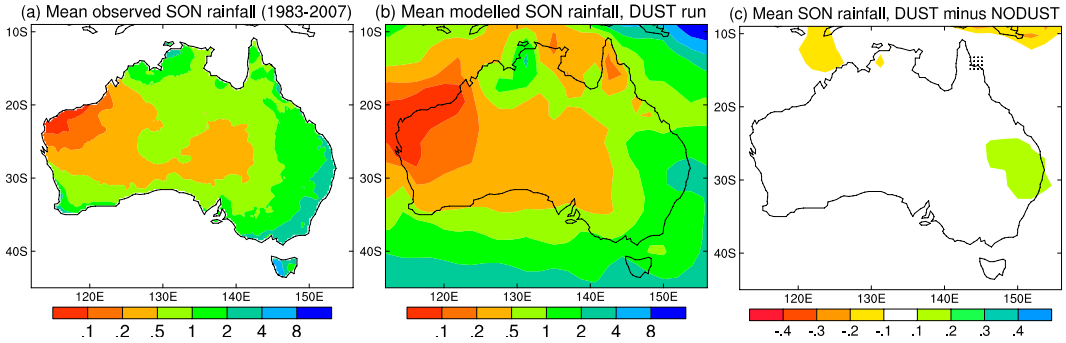

Fig. 5. Mean SON rainfall from **(a)** observations for 1983–2007, **(b)** the DUST run, and **(c)** the difference between the DUST and NODUST runs (in mm per day). In panel **(c)** , stippling shows the (single) grid box where differences are significant at 5%.

ACPD
11, 1595–1639, 2011

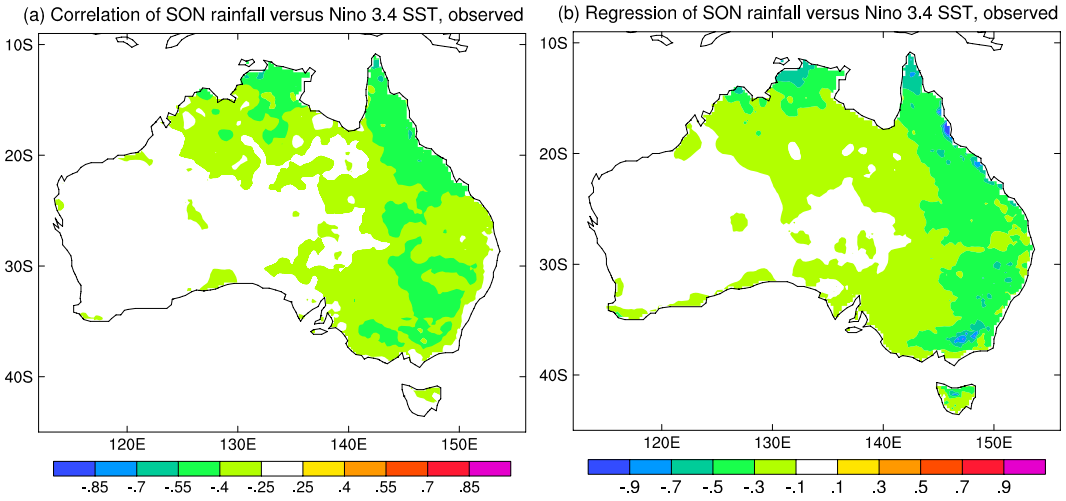

Fig. 6. Observed relationships between Niño3.4 SST and Australian rainfall during SON for the period 1901–2007: **(a)** correlations and **(b)** linear regression (in mm per day per Kelvin).

ACPD
11, 1595–1639, 2011

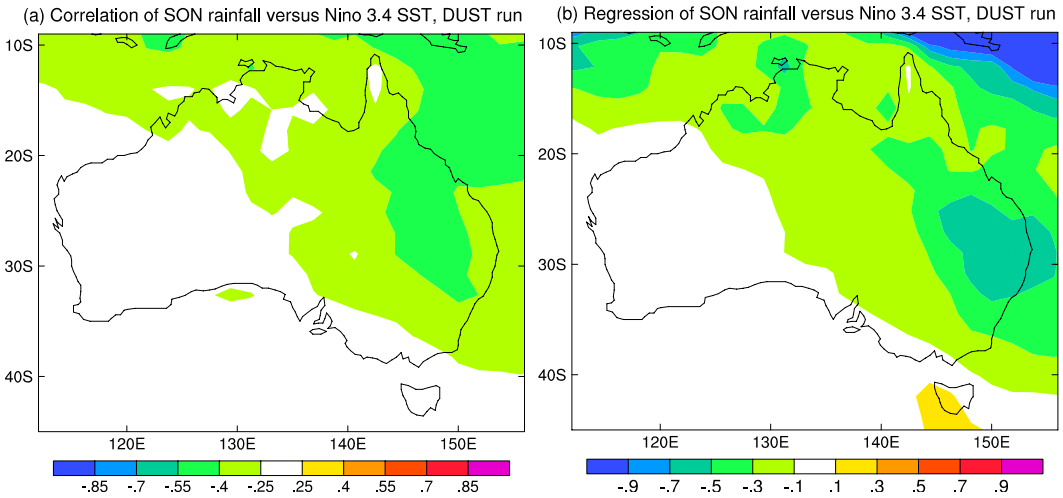

Fig. 7. Modelled relationships between Niño3.4 SST and Australian rainfall during SON in the DUST run: **(a)** correlations and **(b)** linear regression (in mm per day per Kelvin).

ACPD
11, 1595–1639, 2011

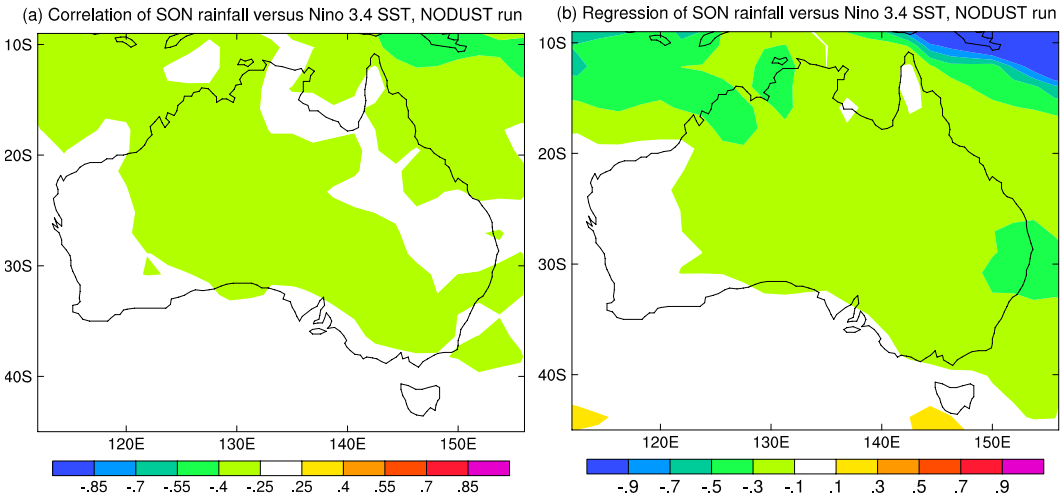

Fig. 8. Modelled relationships between Niño3.4 SST and Australian rainfall during SON in the NODUST run: **(a)** correlations and **(b)** linear regression (in mm per day per Kelvin).

ACPD
11, 1595–1639, 2011

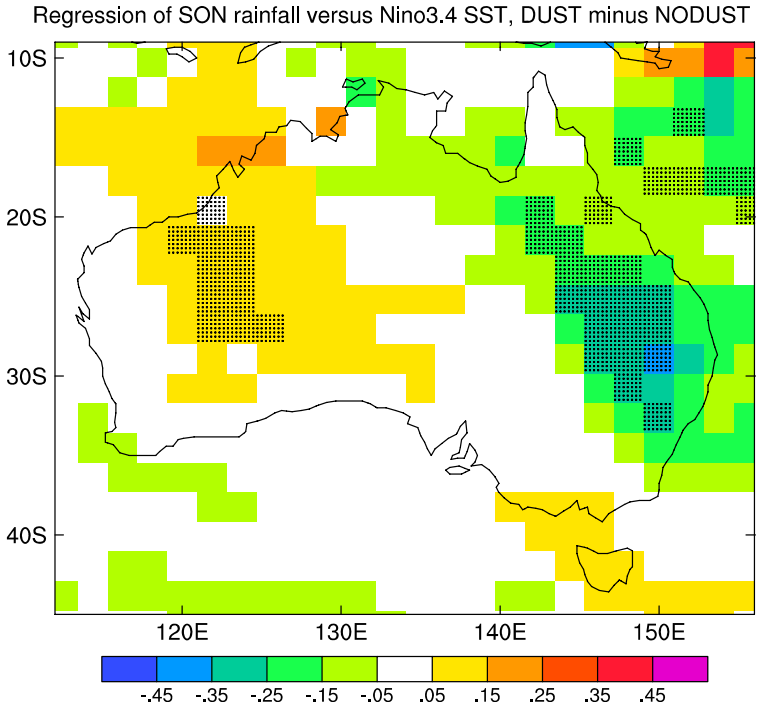

Fig. 9. Difference of the Niño3.4 SST – rainfall regression slopes between the DUST and NODUST runs for SON. Stippled regions are significant at 5%.

ACPD
11, 1595–1639, 2011

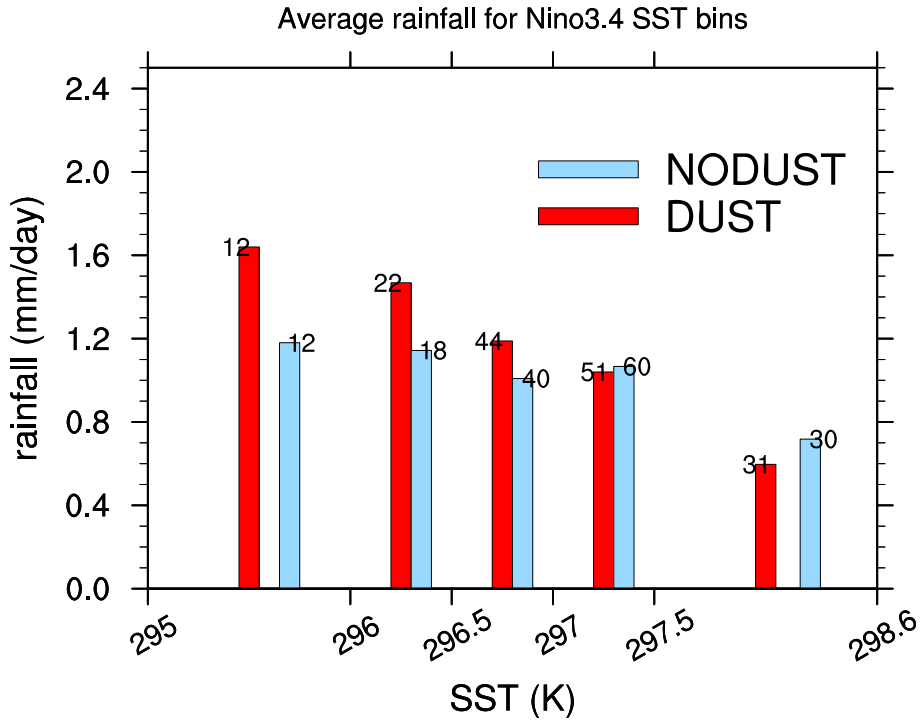

Fig. 10. Rainfall for Niño3.4 SST bins, averaged over the stippled points in eastern Australia from Fig. 9. Red bars are from the DUST run, and blue bars are from the NODUST run. The number of points in each SST bin is shown near the top of each bar. The width of each SST bin is 0.5°, except for the first and last bins, which have width of roughly 1°.

ACPD
11, 1595–1639, 2011

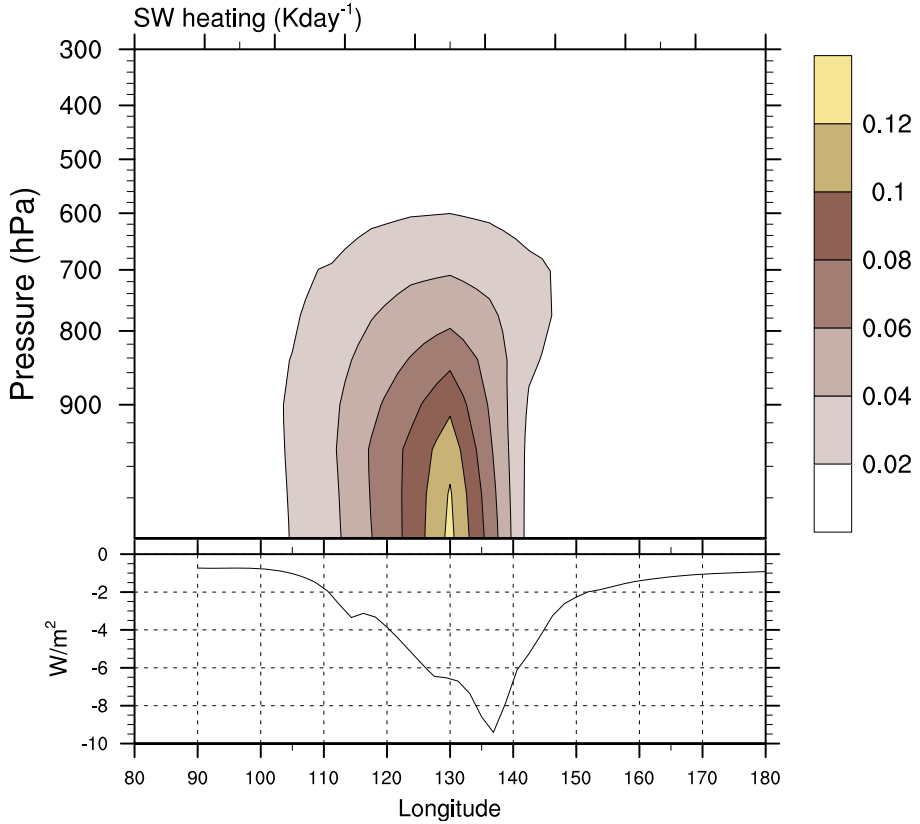

Fig. 11. Dust shortwave radiative forcing for SON, averaged over the latitude range 20.5° S to 29.8° S. The upper panel shows dust atmospheric heating in K $(day)^{-1}$. The lower panel shows dust radiative forcing at the surface in W m^{-2}.

ACPD
11, 1595–1639, 2011

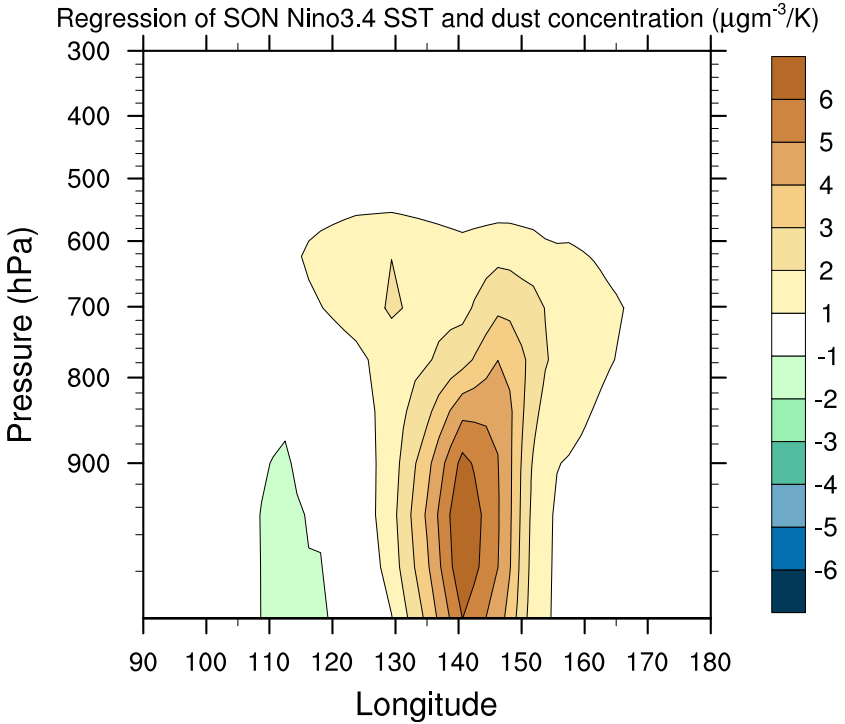

Fig. 12. Regression of SON dust concentration against Niño3.4 SST in the DUST run (in $\mu g\,m^{-3}\,K^{-1}$), averaged over the latitude range 20.5° S to 29.8° S.

ACPD
11, 1595–1639, 2011

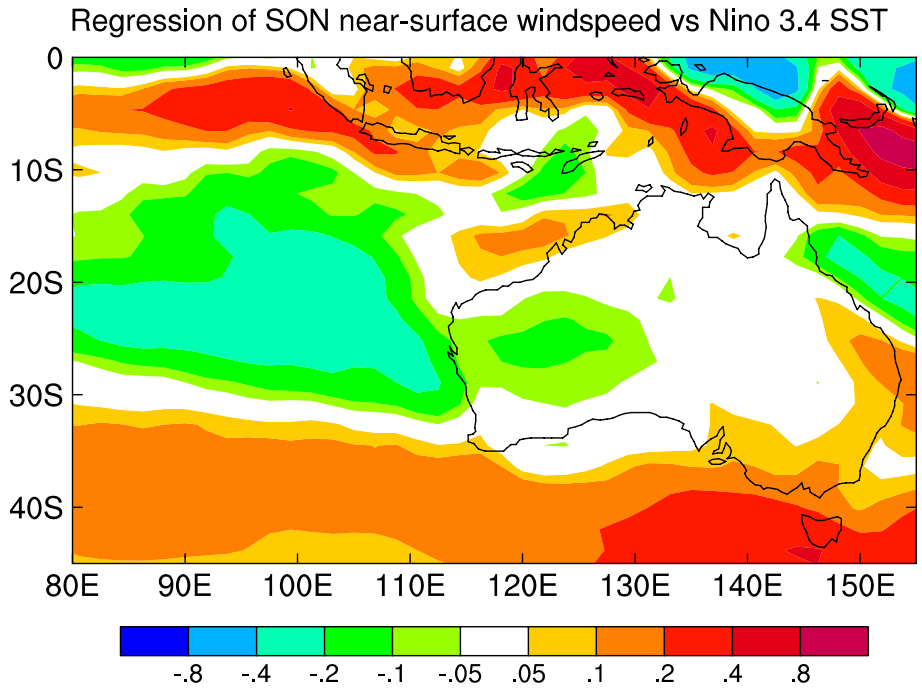

Fig. 13. Regression of SON near-surface wind speed against Niño3.4 SST in the DUST run (in $m\,s^{-1}\,K^{-1}$). Wind speed is calculated at each time step from the vector winds at the lowest model level (approximately 40 m above the surface).

ACPD
11, 1595–1639, 2011

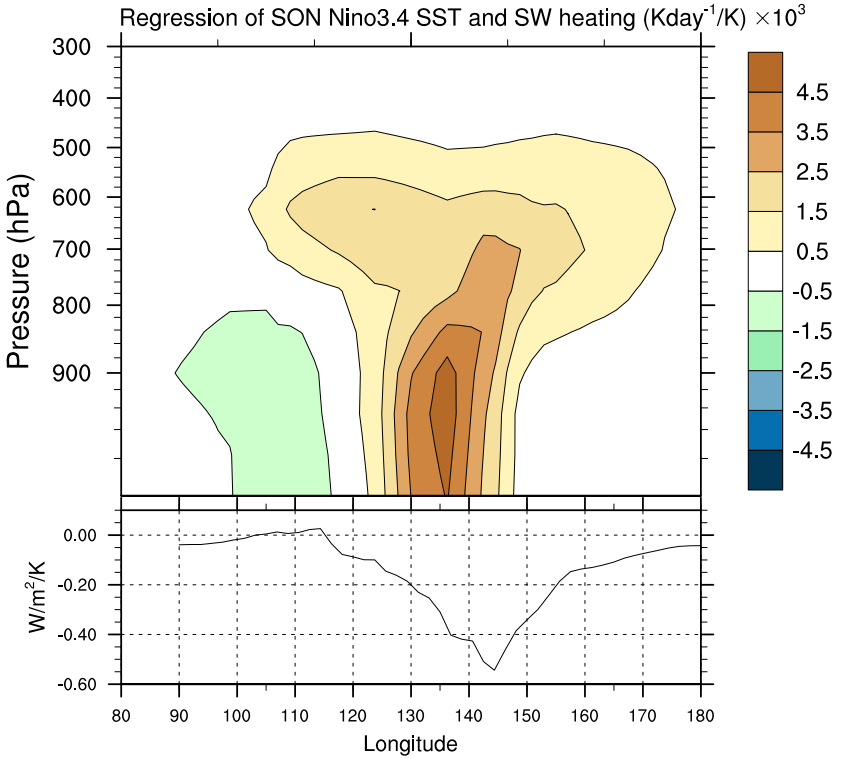

Fig. 14. As Fig. 12, except that dust shortwave radiative forcing is shown instead of dust concentration. The upper panel shows the regression of dust atmospheric heating against Niño3.4 SST in $1000 \times \mathrm{K\,(day)^{-1}\ K^{-1}}$. The lower panel shows the regression of dust surface radiative forcing against Niño3.4 SST in $\mathrm{W\,m^{-2}\,K^{-1}}$.

ACPD
11, 1595–1639, 2011

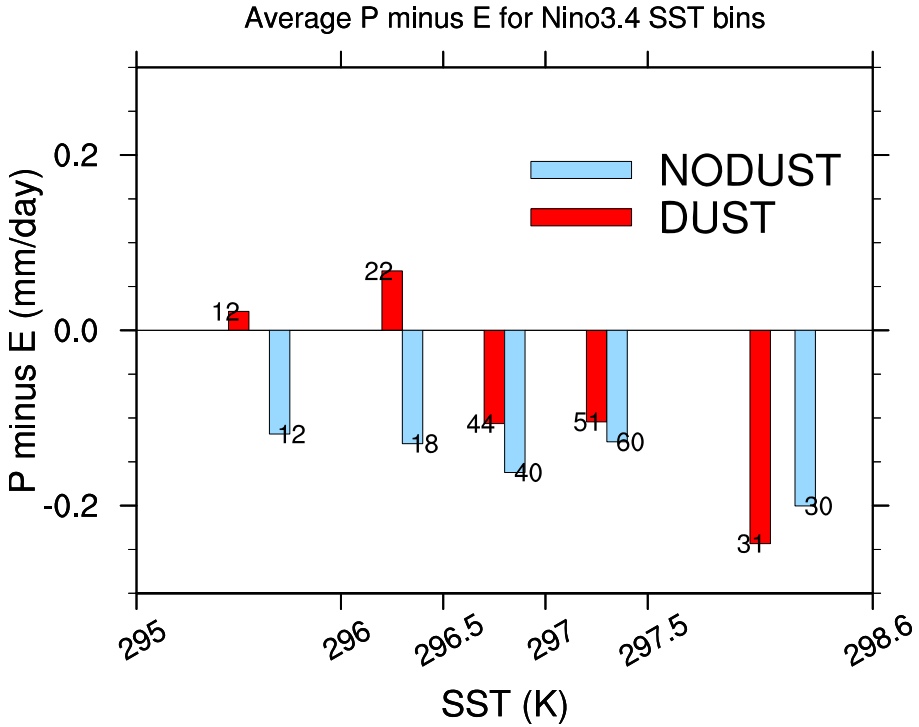

Fig. 15. As Fig. 10, except that *P* minus *E* is shown.

ACPD
11, 1595–1639, 2011